Journal of the Mechanics and Physics of Solids 57 (2009) 32–50

Contents lists available at ScienceDirect

Journal of the Mechanics and Physics of Solids

journal homepage: www.elsevier.com/locate/jmps

The role of the weakest-link mechanism in controlling the plasticity of micropillars

Jaafar A. El-Awady *, Ming Wen, Nasr M. Ghoniem

Mechanical and Aerospace Engineering Department, University of California, Los Angles, CA 90095-1597, USA

ARTICLE INFO

Article history:
Received 29 February 2008
Received in revised form
16 August 2008
Accepted 7 October 2008

Keywords:
Size effects
Dislocations dynamics
Plasticity
Micropillars
Nickel

ABSTRACT

We present a computational study on the effects of sample size on the strength and plastic flow characteristics of micropillars under compression loading. We conduct three-dimensional simulations using the parametric dislocation dynamics coupled with the boundary element method. Two different loading techniques are performed. The plastic flow characteristics as well as the stress–strain behavior of simulated micropillars are shown to be in general agreement with experimental observations. The flow strength versus the diameter of the micropillar follows a power law with an exponent equal to −0.69. A stronger correlation is observed between the flow strength and the average length of activated dislocation sources. This relationship is again a power law, with an exponent −0.85. Simulation results with and without the activation of cross-slip are compared. Discontinuous hardening is observed when cross-slip is included. Experimentally observed size effects on plastic flow and work-hardening are consistent with a "weakest-link activation mechanism".

1. Introduction

Classical continuum mechanics of plasticity is size-independent, and adequately describes the behavior of materials in large structures. However, with the emergence of nano- and microtechnologies, it is recognized that some material properties are dependent on one or more of the dimensions of the solid. Recently, the dependence of strength and ductility on size has been shown in numerous experiments. A "size effect" is defined as a change in a material property due to change in one or more of the dimensions of the physical volume. Within the context of plasticity, one would be interested in understanding how plastic flow characteristics (e.g. strength, hardness, ductility, temporal evolution, etc.) depend on the system size. In recent years, it has been realized that plastic flow in small volumes requires higher stresses than what would be expected in bulk materials.

In recent years, Uchic et al. (2003) developed a test methodology based on a combination of focused ion beam (FIB) machining and a simple extension of the nanoindentation technique. Influenced by this testing methodology, a number of experimental studies have recently been carried out to explore the plasticity size-dependence and the behavior of single-crystal micropillars. In these studies, compression tests were performed on Ni (Uchic et al., 2004; Dimiduk et al., 2005; Maaß et al., 2007a; Shan et al., 2007; Frick et al., 2008), Ni-based superalloys (Uchic et al., 2004; Uchic and Dimiduk, 2005) Cu (Kiener et al., 2006), Mo (Bei et al., 2007b; Greer et al., 2008), and Au (Greer et al., 2005; Greer and Nix, 2006; Volkert

* Corresponding author. Tel.: +1 310 351 7997; fax: +1 310 206 4830.
E-mail address: jelawady@ucla.edu (J.A. El-Awady).

0022-5096/$ - see front matter © 2008 Elsevier Ltd. All rights reserved.
doi:10.1016/j.jmps.2008.10.004

and Lilleodden, 2006; Maaß et al., 2007b; Budiman et al., 2008) single-crystal micropillars having diameters in the range of submicrons to tens of microns, and with a length to diameter ratio in the range 2:1 to 5:1.

These experiments revealed outstanding observations, and most importantly the dependence of the flow strength on the diameter. It was shown that the flow stress exhibits a strong size-dependency, with the smallest specimens (i.e. in the submicron range) having a flow stress that is an order of magnitude higher than bulk specimens. Another common observation is that the flow strength does not scale with the dislocation density (i.e. Taylor Hardening). However, experimental observations of work-hardening dependence on micropillar size and crystal rotation observations are not totally consistent at the present time.

Dimiduk et al. (2005) performed compression experiments on Ni micropillars having sizes in the range of 1.0–40.0 μm and oriented for single-slip. They observed a transition from "bulk-like" to "multiplication-limited" behavior on both the flow strength and the work-hardening at a micropillar size of 20 μm. In addition, for micropillars below 10 μm the deformation is dominated by large strain bursts and that very low work-hardening is observed at high strains. From these results, they suggested that stochastic effects such as dislocation generation by a stress-dependent source distribution, dislocation trapping, and dislocation escape at free surfaces would affect the mobile dislocations and source densities, and in turn would result in the observed size effects.

On the other hand, Greer et al. (2005) performed compression experiments on Au single-crystal micropillars, with sizes in the range of 0.3–7.5 μm. Their results indicate a strong size effect on the flow strength of their tested micropillars. They also observed multiple-slip deformation and essentially no work-hardening in all their micropillars. The exceptionally high strength of these micron-sized single-crystals was interpreted by Greer et al. (2005) and Greer and Nix (2006) to result from dislocation starvation. This concept arises due to dimensional constraints which restrain multiplication of dislocations and thus high stresses would be required to nucleate dislocations either in the bulk or from free surfaces.

Volkert and Lilleodden (2006) also performed compression experiments on Au micropillars having sizes in the range 0.18–8 μm. They observed both single-slip and multiple-slip deformation, and neither affects the inverse relationship between the flow strength and the diameter. In contrast to other experiments, they reported a significant increase in work-hardening as the size of the micropillar decreases. They explained their observations on the basis of a dislocation source-limited mechanism. The main idea here is that an overall decrease in the dislocation density is expected for smaller micropillars and thus an increase in the applied stress is necessary to nucleate or activate new dislocation sources.

This observed increase in work-hardening with a decrease in the micropillar size was confirmed by more recent experiments on Ni by Frick et al. (2008), where they have shown a dramatic increase in work-hardening as the micropillar size decreases. By comparing their results with previous experimental studies, they concluded that work-hardening is a function of both orientation and sample size. Based on TEM observations of the microstructure, they suggested that dislocation pile-ups at the pillar base may play a significant role in controlling work-hardening. Thus, they proposed that the observed increase in work-hardening is due to a combination of dislocation–dislocation interactions and increased stress required to activate dislocation sources with decreasing pillar size. Finally, they also reported a slight pillar rotation and bending of TEM lamellas due to residual stresses which might contribute to the increase in work-hardening.

Micropillar compression experiments using *ex situ* and *in situ* Laue diffraction (Maaß et al., 2007a), have revealed that the FIB fabrication process of micropillars results in preexisting strain gradients that may play an important role in the observed strengthening by the activation of geometrically unpredicted slip systems during loading. These experiments have also revealed that, in contrast to what was previously assumed, crystal rotations do occur during deformation. In contrast to these results, Budiman et al. (2008) used a synchrotron white-beam X-ray submicron diffraction, to study a submicron single-crystal Au micropillar before and after plastic deformation. They concluded that there is no evidence of lattice rotation or lattice curvature caused by the deformation. Thus, they argued that plasticity in single-crystal micropillars is not controlled by strain gradients, but rather by dislocation source starvation.

Kiener et al. (2006, 2007) used Auger electron spectroscopy and transmission electron microscopy to investigate the surface damage due to Ga^+ ion bombardment during FIB sample machining of Cu single-crystals. These experiments revealed that the FIB process results in a region of high dislocation density near the surface that may alter the mechanical properties of the material being tested. On the other hand, Shan et al. (2007) performed *in situ* TEM compression experiments on Ni single-crystal micropillars. They observed a high density of initial defects after FIB processing, which is shown to be driven out of the crystal by compression loading for micropillars having sizes below 0.16 μm, while for larger micropillars, this initial dislocation density is not completely driven out.

Because of the wide-range of such experimental observations, computer simulations may provide useful insights in understanding the origins of experimentally observed size effects. A number of two-dimensional (2-D) and three-dimensional (3-D) dislocation dynamics (DD) simulations have recently been performed to assess the mechanisms associated with the wide range of observations that we discussed earlier. Deshpande et al. (2005) conducted 2-D compression and tension DD simulations of planer single-crystals that incorporate constitutive rules, with consideration of finite deformation. In their study, they considered two types of boundary conditions where the tensile axis is either constrained or allowed to rotate. Their study concluded that the main features of the size dependence are revealed by small-strain analysis. In a similar study, Benzerga and Shaver (2006) performed 2-D small-strain simulations that explicitly incorporated length and time scales associated with dislocation nucleation. From their results, they concluded that the apparent strengthening is due to internal stresses and the dislocation source length variation. This work was further extended by Guruprasad and Benzerga (2008) who performed 2-D simulations with a high initial dislocation density of

$\rho = 1.5 \times 10^{14}\,\mathrm{m}^{-2}$. They showed that even at such high densities, Taylor hardening does not hold. In addition, they proposed that the increased hardening rate of smaller specimens is mainly due to dislocation junction formation. Although this may serve as an alternative mechanism to explain the observed increase in hardening, it requires a much higher initial source density (about two orders of magnitude higher than typical experimental observations Greer et al., 2005; Dimiduk et al., 2005. It should be noted here that although such 2-D DD simulations give useful insight, they are still based on a number of idealizations that need to be confirmed by 3-D simulations. For instance, the effects of cross-slip, dislocation bowing and other key dislocation interaction mechanisms are either totally ignored or added in an ad hoc manner. The usefulness of 2-D simulations will be extended when calibrated with results from 3-D simulations.

Tang et al. (2007) performed 3-D discrete DD simulations that neglect the boundary conditions of the micropillars. Based on these simulations, it is argued that the escape of mobile dislocations in smaller micropillars is faster than in larger ones. Thus, as the micropillar size gets smaller, the mobile dislocation density becomes smaller. This leads to an increase in the resistance to plastic flow and thus the observed size effects. Weygand et al. (2007) also performed 3-D simulations that accounted for traction free boundary conditions using the finite element method (FEM). Due to the heavy calculations needed to perform the simulations and the difficulty in dealing with complex geometries, detailed analyses were limited. To overcome such computational difficulties, El-Awady et al. (2008) developed a self-consistent formulation of 3-D parametric dislocation dynamics (PDD) with the boundary element method (BEM) to incorporate the influence of free and internal interfaces on dislocation motion, and hence to describe microplastic flow in finite volumes. They performed large scale simulations using this method and have shown that in contrast to 3-D models that ignore surface effects, image fields arising from the finite geometry of micropillars have an important effect on the dislocation microstructure, especially for micropillars having submicron diameters. In addition, they showed that for small size single-crystals, the flow stress is not controlled by dislocation–dislocation interaction, as in the case of bulk crystals, but rather controlled by the activation of the weakest dislocation links trapped at the surface. This is in agreement with the statistical examination of the mathematical model developed by Parthasarathy et al. (2007). In their work they developed an analytical model that assumes a random distribution of pins in the sample, with each pin having a dislocation arm starting from it and ending at the surface. This model calculates the longest of the arms each of which has a length that is the shortest from a pin to the surface, and thus will give the lower bound on the athermal CRSS in the microstrain regime. They then evaluated the statistics of placing a fixed number of pins randomly on an oblique cylinder section using a random number generator. From these simple calculations it was concluded that the observed size effects are based on a statistical variation of the dislocation source lengths.

Recently, Tang et al. (2008) performed DD simulations of single-crystal micropillars containing initial dislocation Frank net structure by annealing a collection of jogged and straight dislocations under zero loads. They show that the observed plastic deformation from their simulations is caused by the operation of single junction-stabilized spiral sources, and is followed by intervals of purely elastic straining when the sources are shut-down. Although in their study the initial dislocation densities are two orders of magnitude higher than those reported by experimental studies (Greer et al., 2005; Dimiduk et al., 2005), and they do not provide any rationalization of experimentally observed statistical variations in the observed flow strength or work hardening, their results provide insight into a mechanism that may be responsible for the experimentally observed staircase stress–strain behavior.

In the present work, the objective is to explore, via statistical analysis from computer simulations, the effect of specimen size on plastic flow and work-hardening. We perform 3-D DD simulations of Ni single-crystal micropillars under compressive loading. The simulations are carried out using the framework developed by El-Awady et al. (2008). In these simulations, micropillars are oriented for multi-slip and compressive loading is applied at a constant applied strain rate. In addition, simulations with and without the activation of cross-slip are performed. Comparison of the results in both cases are made to study the influence of cross-slip on plasticity in small volumes.

The organization of this paper is as follows. First, we present a brief outline of the computational method in Section 2. In Section 3, the setup of computer simulations is explained, and the 3-D simulation results of the size effect on the flow strength and work-hardening are presented and discussed in Sections 4 and 5, respectively. In addition, the temporal characteristics of plastic flow are examined using the fast Fourier transform (FFT). Finally, discussion and conclusions are given in Section 6.

2. Computational method

The computational method adopted here follows the formulation developed by El-Awady et al. (2008). In this formulation, the BEM is coupled with the 3-D PDD formulation to incorporate the influence of free and internal interfaces on dislocation motion, and hence to describe microscopic plastic flow in finite volumes. Here, we briefly review some of the important features of the BEM-PDD method, while detailed information about the method can be found elsewhere (El-Awady et al., 2008; Takahashi and Ghoniem, 2008; Ghoniem et al., 2000; Ghoniem and Sun, 1999).

In this methodology, the effects of surfaces and boundary conditions are modelled with the BEM, while the computational structure of the PDD is unchanged. In the PDD, all dislocation loops are discretized into curved parametric segments and the elastic field, forces, and motion of the dislocation segments in an infinite medium are computed. Following the superposition method developed by Van der Giessen, Needleman and co-workers (Van der Giessen and

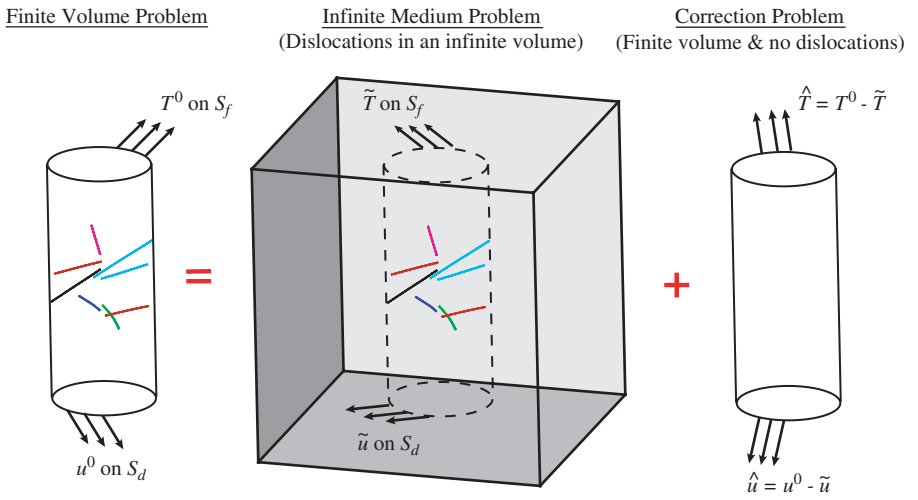

Fig. 1. Scheme of the superposition representation for the micropillar.

Needleman, 1995) to introduce boundary conditions in discrete DD, the total displacement and stress fields are given as

$$u_{ij} = \tilde{u}_{ij} + \hat{u}_{ij},$$

$$\sigma_{ij} = \tilde{\sigma}_{ij} + \hat{\sigma}_{ij}, \tag{1}$$

where the ($\sim$) fields are the elastic fields in an infinite medium resulting from all dislocation loops, while the ($\wedge$) fields are the *image fields* that enforce the boundary conditions. This scheme is demonstrated in Fig. 1.

To evaluate *image fields* due to external or internal surfaces, the following four steps need to be performed. First, the elastic stress field in an infinite medium resulting from all dislocation loops is evaluated. Tractions at the surfaces of the finite crystal due to this stress field are then determined, reversed and placed on the surface as traction boundary conditions. These traction boundary conditions in addition to any imposed constraints are employed in BEM to calculate all unknown surface tractions and displacements. Finally, the image stress field is calculated, and the result is superimposed as indicated in Eq. (1). Once the dislocation stress field and the image stress field are obtained, the total stress and hence the total force on each dislocation can be computed.

Thus, the evolution of the microstructure can be obtained using the framework of the PDD method, were the equations of motion for the dislocation loops involve dislocation drag and interaction with other dislocations within the simulation volume, and are developed in the following computational form

$$\mathbf{K}\frac{\mathrm{d}\mathbf{Q}}{\mathrm{d}t} = \mathbf{F}, \tag{2}$$

where $\mathbf{K}$ is a stiffness matrix, $\mathbf{Q}$ are generalized coordinates, and $\mathbf{F}$ force vector (for details, see reference (Ghoniem et al., 2000).

3. Problem setup

The simulations carried out in this work are to study the behavior of face-centered-cubic (FCC) single-crystal micropillars oriented for multiple-slip. In all calculations, crystal properties are taken to be that of nickel with a shear modulus $\mu = 76\,\mathrm{GPa}$, Poission's ratio $\nu = 0.31$, lattice parameter $a = 0.3524\,\mathrm{nm}$, and Burgers vector magnitude of $b = 0.1246\,\mathrm{nm}$. In addition, micropillar diameters are varied from $D = 0.25$ to $5.0\,\mu\mathrm{m}$ and the aspect ratio for all calculations is fixed at $L : D = 3 : 1$. A schematic of the simulated micropillars is shown in Fig. 2. The initial dislocation densities are varied from $\rho = 1 \times 10^{12}$ to $50 \times 10^{12}\ \mathrm{m}^{-2}$.

Dislocation segments observed in TEM are part of a network and are connected to other segments by junctions. Foreman (1967) showed that the change in the activation stress of a Frank–Read source due to the stress field of the side-arms is small. This was then supported by DD simulations that showed that the increase in flow stress due to the side-arms, acting as additional obstacles for moving dislocations, is smaller than the error due to different starting configurations (von Blanckenhagen et al., 2004). On the other hand, Schoeck and Frydman (1972) showed that in a random dislocation forest, the stress to overcome the junctions is higher for screw dislocations than for edges, although exact values depend on the nature of the forest (Basinski and Basinski, 1979; Puschl et al., 1982). In addition, 20% of the dislocation junctions are strong enough to be permanent pinning points and arrest dislocation motion.

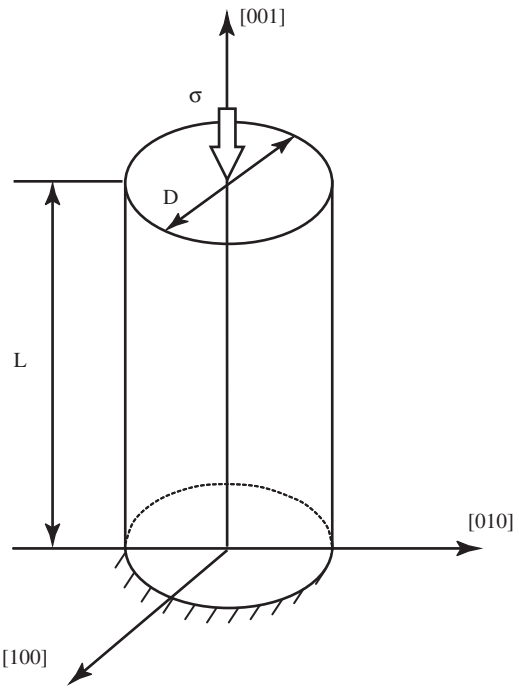

Fig. 2. Schematic of the simulated single-crystal micropillar oriented in the [001] direction. The micropillar is loaded axially in compression along the [001] direction. A constant aspect ratio of $L:D=3:1$ was used for all simulations.

A point that is still unclear and unevaluated in literature is the spacing between strong-dislocation obstacles that pin dislocations and the initial dislocation distribution in micropillars. Clear evidence of dislocation pinning and strong-dislocation obstacles can be observed in TEM observations of bulk Cu deformed in tension (Mughrabi, 1976). In addition, clear experimental observations show that there exist strong-dislocation obstacles (dislocation pinning points) in compressed micropillars. Recently, Norfleet et al. (2008) examined cut foils from 1, 2, 5, 10 and 20 μm pillars and have demonstrated a deformation structure that is qualitatively similar to those formed within macroscopic samples experiencing Stage I glide. In addition, Shan et al. (2007) showed that Ni microcrystals as small as 300 nm can sustain a dislocation structure under stresses as high as 2.6 GPa, which is inconsistent with the dislocation starvation hypothesis. Although, the probability that a "starvation-like" concept could apply for sizes smaller than 300 nm, it cannot be ruled out since in the same study it was shown that a 150 nm diameter Ni microcrystal appears to be dislocation free before and after deformation. Based on such experimental evidences we believe that having a distribution of FR sources and single pinned dislocations is acceptable and is in fact representative of the real dislocation structure in compressed micropillars.

In our current simulations, we represent the dislocation network by randomly distributed FR sources and single-ended surface dislocations on different slip planes in the bulk of the crystal, and we neglect the side-arms, which would lie on secondary slip planes. Single-ended surface dislocations are dislocations that are pinned from one end in the bulk, while the other end lays on the surface of the crystal. The center of each slip plane of each dislocation is generated at random such that all planes do not intersect the top or bottom of the micropillar. The initial length of each FR source or single-ended surface dislocations, λ, is calculated based on a two-parameter Weibull distribution, having the following probability density function (PDF):

$$f(\lambda)=\frac{\beta}{\theta}\left(\frac{\lambda}{\theta}\right)^{(\beta-1)}\mathrm{e}^{-(\lambda/\theta)}\quad\text{for }\lambda\geqslant 0, \tag{3}$$

where $\beta>0$ is the shape parameter and $0<\theta<D$ is the scale parameter or the mean of the distribution lengths. Thus, by choosing a random number, u, from the uniform distribution in the interval $[0,1]$, a Weibull distribution of the dislocation source length can be obtained as follows:

$$\lambda=\theta(-\ln(u))^{1/\beta}. \tag{4}$$

To study the effects of the statistical variation of the initial dislocation distribution on the plastic response of the crystal, four different Weibull distribution realizations were chosen. The PDF of these four realizations are shown in Fig. 3.

In all simulations, a uniform compressive load in the [0 0 1] direction is imposed on the top surface of the cylinder while the bottom surface is kept fixed. This compression loading is performed by two techniques: a high-load sensitivity

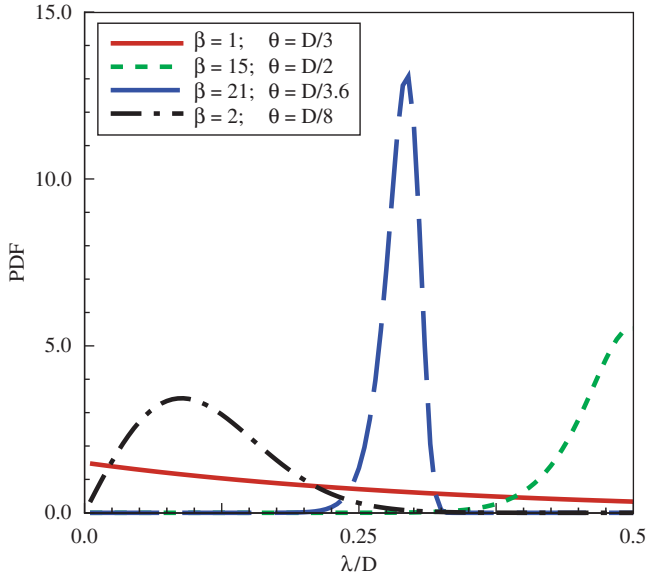

Fig. 3. Probability density function (PDF) of the dislocation length to the micropillar diameter ratio.

technique and a low-load sensitivity technique. In the high-load sensitivity technique, the compression loading is performed under a constant strain rate $\dot{\varepsilon} = 200\,s^{-1}$. Thus, the rate of loading is set by this strain rate such that

$$\dot{\sigma} = E(\dot{\varepsilon} - \dot{\varepsilon}^p), \tag{5}$$

where $\dot{\varepsilon}^p$ is the plastic strain rate that is obtained from the motion of the dislocations as follows:

$$\dot{\varepsilon}^p = -\frac{1}{2V}\sum_{i=1}^{N_{tot}} l^i v^i (\mathbf{n}^i \otimes \mathbf{b}^i + \mathbf{b}^i \otimes \mathbf{n}^i), \tag{6}$$

where V is the volume of the simulated crystal and N_{tot} is the total number of dislocation segments. In addition, l^i is the length of dislocation segment i, having a velocity magnitude v^i, a Burgers vector $\mathbf{b}^i$, and a slip plane normal $\mathbf{n}^i$. In this loading technique, the applied load is allowed to decrease during the simulation when the calculated plastic strain rate is greater than the imposed constant strain rate. Therefore, flow-softening (or a negative work-hardening rate) is not suppressed. This loading technique enables us to adjust the applied load to follow the individual behavior of dislocations as they evolve. Currently, no experimental procedure has such high-load sensitivity to be abe to adjust the applied loading based on tracking the time dependence of individual dislocation slip events.

In the low-load sensitivity technique, the same constant strain rate is applied but the applied load is not allowed to decrease during the simulation. To maintain this condition, the calculated plastic strain rate Eq. (6) is compared to the constant applied strain rate and the loading is imposed as follows:

$$\begin{aligned} \dot{\sigma} &= E(\dot{\varepsilon} - \dot{\varepsilon}^p) \quad \text{for } \dot{\varepsilon}^p \leqslant \dot{\varepsilon} \\ &= 0, \quad \text{for } \dot{\varepsilon}^p > \dot{\varepsilon}. \end{aligned} \tag{7}$$

Thus, flow-softening is prevented. This technique is consistent with all experimental studies so far. It should be noted here that the strain rate used in our calculations is 3 orders of magnitude higher that the experimental work. The effect of strain rate on the flow strength was tested and calibrated using a stress controlled loading. In the stress controlled loading, the stress is discretely increased by a 1 MPa loading increment every time the plastic strain rate approaches zero. The results of varying the strain rate on the flow strength for micropillars below 2.5 μm are observed to be minimal for strain rates $1000\,s^{-1}$, and they agree well with the results from simulations using a stress controlled loading. The reason for this is that the stresses reached in these micropillars are so high and the pillars have sufficient dislocation densities that the plastic strain released in these micropillars are much greater than the imposed strain within s specified time interval. The effect of changing the strain rate on the flow strength starts to be observed for pillars having sizes above 2.5 μm, since the stresses reach in these sizes is somewhat lower. Thus, in the current simulations, a strain rate of $200\,s^{-1}$ and a time step of 2.5×10^{-11} s were found to be computationally efficient while being small enough not to have a large effect on the results of the simulated micropillars.

4. Size effects on the flow strength

In this section, we analyze simulation results of the size effects on the plastic flow of micropillars. First we discuss the effects of varying the dislocation link length on the computed flow strength, then we show the influence of the loading sensitivity on the results. Finally, we discuss the role of several parameters on the observed size effects and present a number of scaling laws.

4.1. Dislocation-link length effects

In Fig. 4, the engineering stress–strain relationships of four micropillar sizes $D = 0.25, 0.50, 0.75$, and $1.00\,\mu m$, are shown, respectively. To study the effect of the initial dislocation source length distribution on the flow strength, the length is varied based on the Weibull distribution shown in Fig. 3. The initial dislocation density in these simulations is set to be $\rho = 3 \times 10^{12}\,m^{-2}$. A clear size effect on the flow strength is observed, as well as an overlap of the results from different sizes. In addition, as in the experimental observations, a substantial scatter in the flow strength from different simulations is observed.

It is observed that the main factor controlling this scatter is the scale parameter, θ, (i.e. mean dislocation source length). When this mean value is close to the radius of the micropillar, a lower bound of the flow strength is calculated for this micropillar size, and as this mean length decreases, the flow strength increases. Thus, it is possible to rationalize the

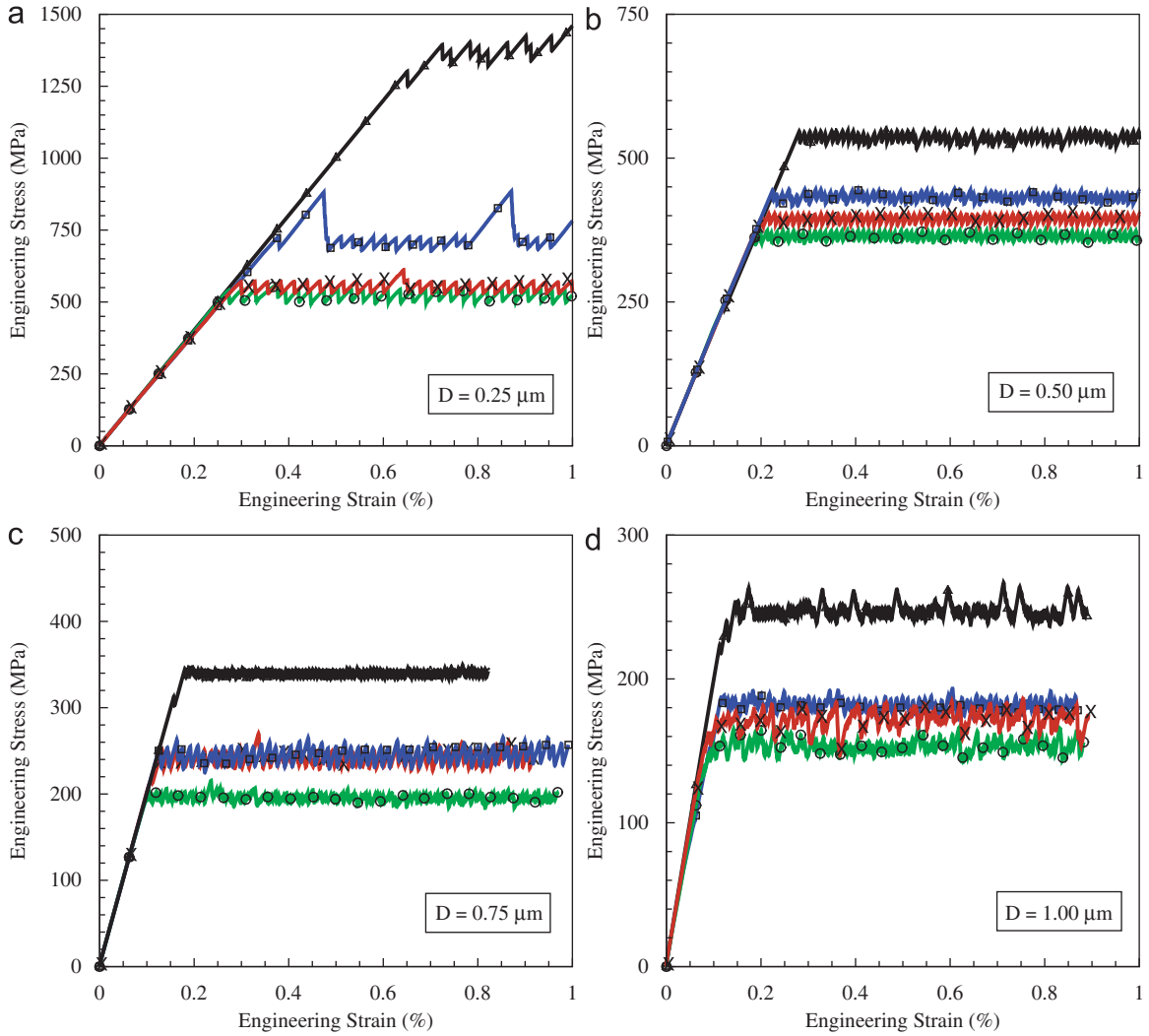

Fig. 4. The engineering stress–strain relationships for different micropillar sizes: (a) $D = 0.25\,\mu m$; (b) $D = 0.50\,\mu m$; (c) $D = 0.75\,\mu m$; (d) $D = 1.00\,\mu m$. The initial dislocation length is based on the Weibull distribution with the following parameters: (–△–) $\beta = 2$ & $\theta = D/8$, (–□–) $\beta = 21$ & $\theta = D/3.6$, (–×–) $\beta = 1$ & $\theta = D/3$, and (–○–) $\beta = 15$ & $\theta = D/2$. The compression simulations are performed using the high-load sensitivity technique.

observed size effect on the basis of the statistical variation of the initial dislocation link length, which is consistent with the mathematical predictions of Parthasarathy et al. (2007).

It should be mentioned here that, although dislocations can initially have lengths that are up to $D\sqrt{3}$ in our current configuration of simulated micropillars, these dislocations expand under loading at lower stresses than the flow strength and eventually get truncated at the surface with lengths below $D/2$. The effect of this on the results will be an initial small step formation in the elastic loading zone after which the material behaves elastically until sources that are smaller than $D/2$ are activated and plastic flow is reached. This behavior was discussed in detail in our previous work (El-Awady et al., 2008) and has no effect on the flow strength. Thus in our current analysis, we limit the initial single-ended dislocation length distribution to be in the effective range $0 \leqslant \theta \leqslant D/2$.

To understand the temporal evolution of the dislocation density, we utilize the FFT. Prominent periodicity can be easily discerned from the FFT, and that may shed light on collective dislocation activities in the form of avalanches. In Fig. 5, the power of the dislocation density, which is the magnitude of the FFT of the dislocation density squared, is plotted against the period for different realizations of the initial dislocation distributions. The peaks that are observed in these plots represent prominent cycles (i.e. dislocation activities) which are periodically repeated.

A number of distinct observations can be seen from these plots. In Fig. 5(a) and (b) a wider range of peaks are observed and thus, a larger number of dislocation activities exist in these micropillars due to the existence of a number of almost equal sized dislocations as indicated from the Weibull distribution. These micropillars are observed to deform by multi-slip. However, the micropillar in (b) is observed to have a larger number of activated slip planes than in case (a), thus, a much wider range of prominent peaks are observed. In Fig. 5(c) and (d), only one prominent peak is observed and thus, only a small number of dislocations are activated in these micropillars and the micropillars deform by single-slip. This is again due to the nature of the "weakest link," or dislocation source link-length distribution. The probability of having a larger dislocation length is small and thus most dislocations are of smaller size. Thus, when the applied load reaches a value high

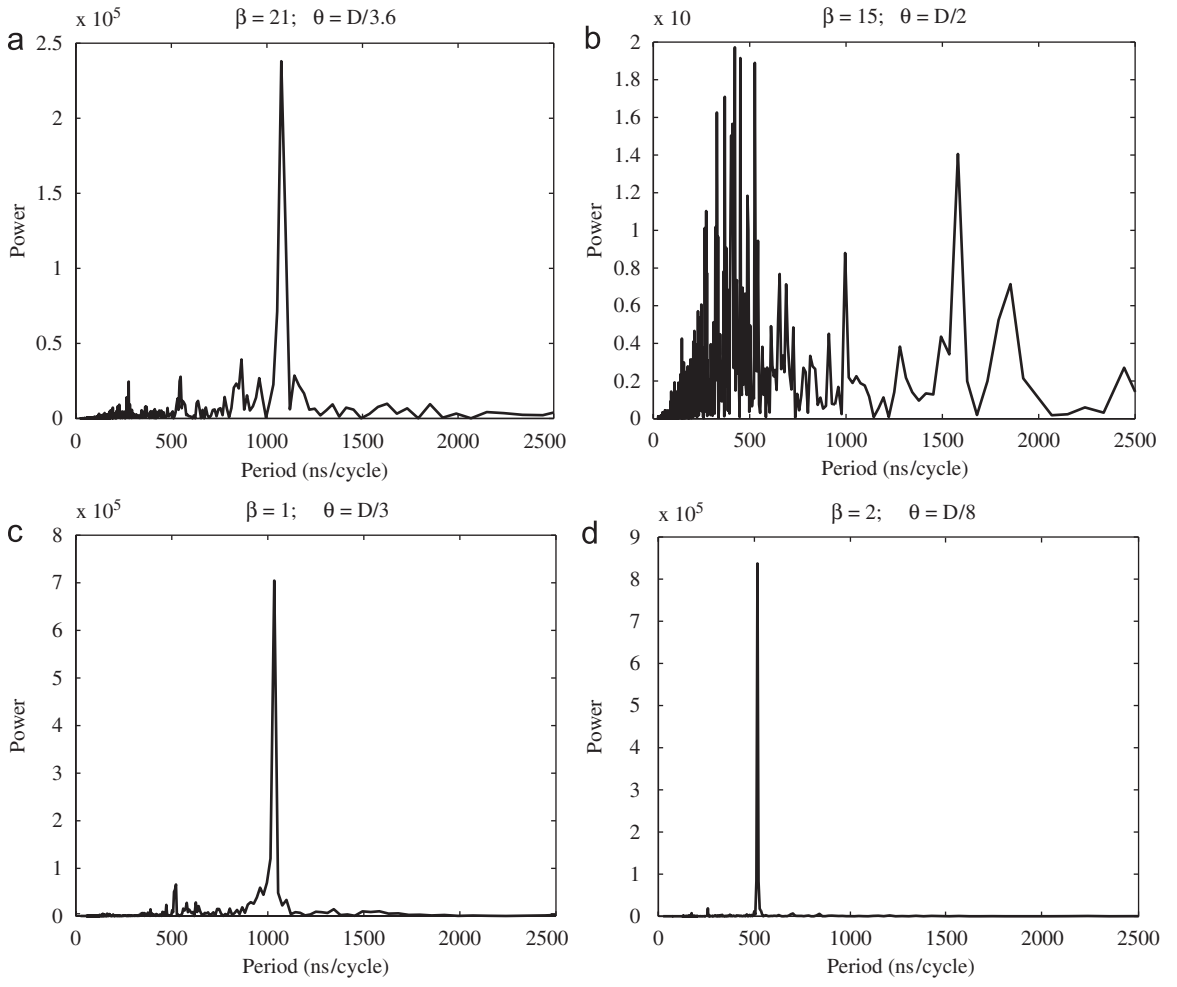

Fig. 5. FFT power versus period for the dislocation density for micropillar size $D = 0.75\,\mu m$ and an initial dislocation distribution with parameters: (a) $\beta = 21$ & $\theta = D/3.6$; (b) $\beta = 15$ & $\theta = D/2$; (c) $\beta = 1$ & $\theta = D/3$; and (d) $\beta = 2$ & $\theta = D/8$.

enough to activate the largest source, only a limited number of dislocation activities are observed. In fact in case (d) only one dislocation is observed to be active.

4.2. Effects of loading sensitivity

Typical engineering stress–strain responses for different micropillar sizes using both loading techniques are shown in Fig. 6. The initial dislocation density for all cases is $\rho = 6.5 \times 10^{12}\,\mathrm{m}^{-2}$ and the initial microstructure for each size in both loading techniques is the same. A clear size effect on the flow stress is observed independent of the loading technique. The flow strength increases as the micropillar diameter decreases, and after the flow strength is reached, essentially no work hardening is observed.

It is interesting to note that, with the same initial microstructure, the flow strength in the low-load sensitivity technique is 10–20% higher than that of the high-load sensitivity technique. This increase is attributed to an increase in the dislocation density when suppressing the applied load from decreasing. This is shown in Fig. 7, where the dislocation density is plotted against the strain for some of the cases show in Fig. 6. As the load is prevented from decreasing, additional dislocation sources are activated, the dislocation density increases which increases dislocation–dislocation interactions and dipole or junction formation and thus a higher stress is needed to activate dislocations. Finally, in both loading techniques at the onset of plastic flow, the dislocation density saturates and thus the observed lack of work-hardening.

In Fig. 8, the FFT power of the dislocation density is plotted versus the period for the two micropillar sizes $D = 0.5$ and $1.0\,\mu\mathrm{m}$. The initial dislocation distributions for the result shown have parameters $\beta = 1$ and $\theta = D/3$. In addition, results from both loading techniques are shown. By comparing the plots from the two different sizes, it is observed that the larger micropillar size has a wider range of peaks or activities. This is mainly because the large size has a higher number of activated sources. By comparison, a larger number of dislocations are activated at low-load sensitivity as compared to high-load sensitivity cases.

4.3. Flow strength scaling laws

To develop flow strength scaling laws, a statistical investigation is performed on the range of diameters from 0.25 to $5.0\,\mu\mathrm{m}$. For each micropillar size, the initial dislocation density is statistically varied from $\rho = 1 \times 10^{12}$ to $50 \times 10^{12}\,\mathrm{m}^{-2}$ and the initial dislocation link length distribution was also statistically varied as discussed in Section 3. Fig. 9 shows the statistical results of the flow strength, σ_f, at 0.5% strain versus a number of parameters. For these results, the high-load sensitivity techniques was employed.

In Fig. 9(a), the flow strength is plotted against the micropillar diameter D. A clear size dependence is observed. In addition, a wide scatter is observed for the flow strength of each size. The scaling relationship for the flow strength, σ_f, with the diameter is a power law of the form

$$\sigma_f = 222.65 D^{-0.69}, \tag{8}$$

where D and σ_f have units of μm and MPa, respectively. The correlation coefficient of the simulated data with this fitting law is calculated to be $r = 0.84$, which signals a large scatter in the flow strength data. This suggests that, in addition to the

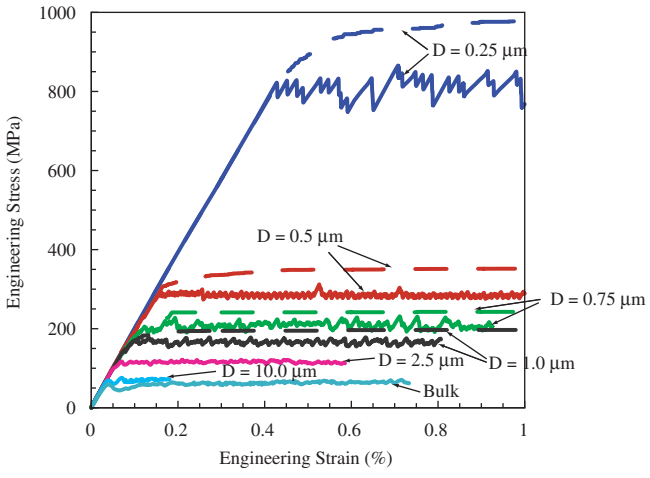

Fig. 6. Engineering stress–strain for compression simulations of different micropillar sizes. Solid lines are for simulations using the high sensitivity loading technique while dotted lines are for simulations using the low sensitivity loading technique.

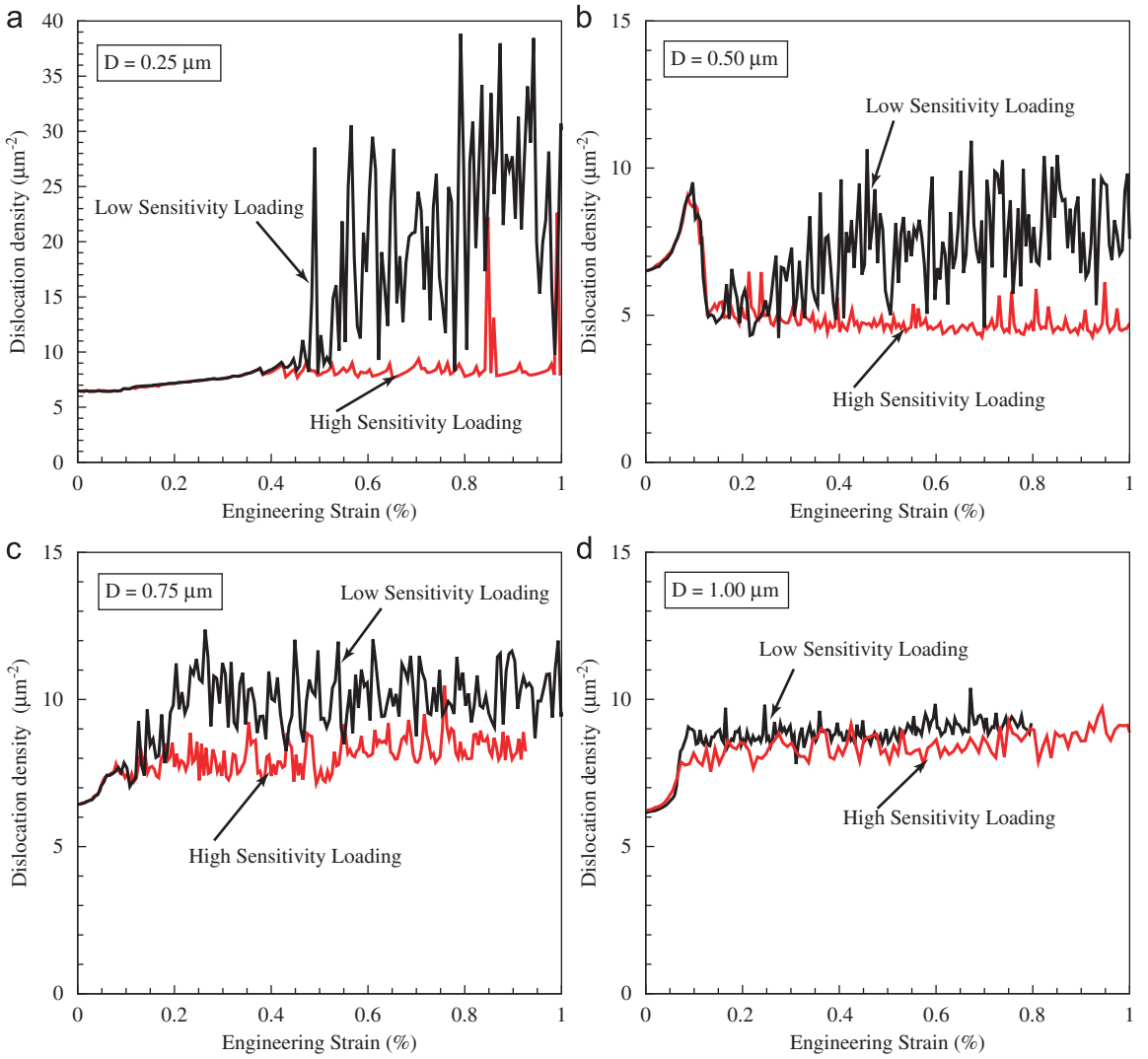

Fig. 7. Dislocation density versus engineering strain for: (a) $D = 0.25\,\mu m$; (b) $D = 0.50\,\mu m$; (c) $D = 0.75\,\mu m$; (d) $D = 1.0\,\mu m$. Red lines are for simulations using the high sensitivity loading technique while the black lines are for simulations using the low sensitivity loading technique.

micropillar size other parameters can be more fundamental than the pillar size. In the following, we will investigate the strength scaling with several other important parameters.

In Fig. 9(b), the flow strength is plotted against the square root of the dislocation density at the onset of plastic flow. It is clear from this figure that the Taylor Hardening law fails in all cases studied here, since there is no obvious correlation between the flow strength and $\sqrt{\rho}$. In Fig. 9(c), the flow strength is plotted against the product of the diameter with the average activated dislocation source length. The best fit in this case is again a power law as follows:

$$\sigma_f = 146.23(D\langle\lambda\rangle)^{-0.41}. \tag{9}$$

The scatter of the data in this case is much smaller than in the relationship with the diameter, and the computed correlation coefficient is $r = 0.94$. By removing the diameter of the micropillar from the relationship we observed a better fit for the data, as shown in Fig. 9(d), where the flow strength is plotted against the average activated dislocation source length, $\langle\lambda\rangle$, for different micropillar sizes. The scaling relationship here is also found to be a power law but with an exponent -0.85. The scatter observed here is much smaller than for the data observed in all previous relationships and the computed correlation coefficient is $r = 0.97$. The best scaling relationship for this data is

$$\sigma_f = 94.93(\langle\lambda\rangle)^{-0.85}, \tag{10}$$

where $\langle\lambda\rangle$ and σ_f have units of μm and MPa, respectively. It should be noted here that the activated dislocation length is in fact strongly dictated by the pillar diameter. Thus, there will be a lower bound for any pillar size when the average dislocation length is equal to the radius of the pillar. The upper bound, on the other hand, would be the case when the pillar

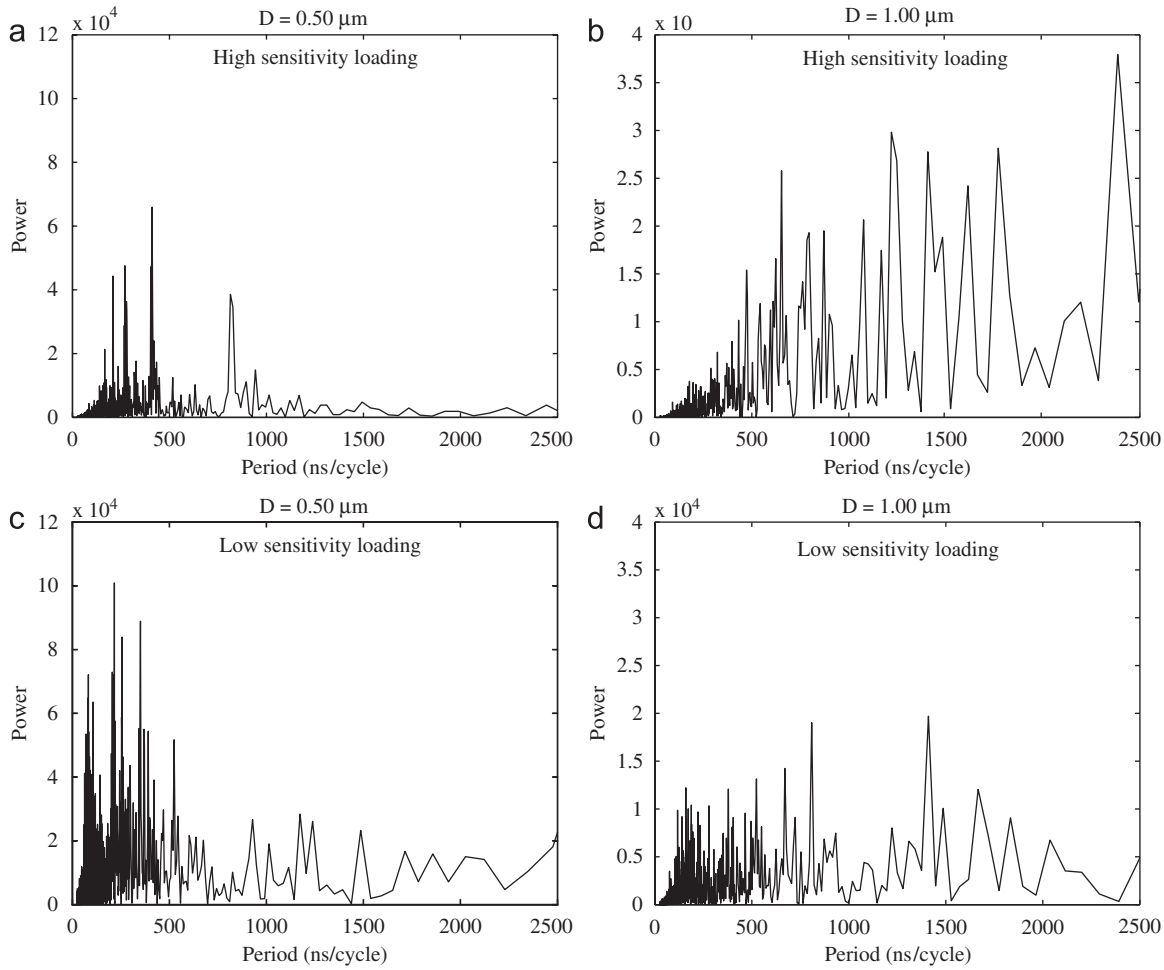

Fig. 8. FFT power versus period for the dislocation density of micropillar sizes $D = 0.5$ and $1.0\,\mu m$, respectively. In (a) and (b), the high-load sensitivity technique is applied, while in (c) and (d) the low-load sensitivity techniques is applied.

is free from dislocations. In this case, the flow strength would be the theoretical strength required to nucleate dislocations either from the bulk of the pillar or most likely from the surface (Zhu et al., 2008).

Experimental results from both Dimiduk et al. (2005) and Frick et al. (2008) are plotted in Fig. 10 as open diamond and open circle symbols, respectively. The results from the Weibull distribution with parameters $\beta = 21$ and $\theta = D/25$ are also plotted in Fig. 10 as solid circle symbols. From our simulations, the Weibull distribution with these parameters is shown to give flow strengths that fall in the middle of the range of experimentally observed flow strengths. It should be mentioned that the corresponding mean value of $\lambda = D/25\,\mu m$, indicating that dislocation segments with link-length comparable to the pillar diameter are rare. For sizes below $D = 1.0\,\mu m$ and distributions with the parameters given in Fig. 3, the computed flow strengths are observed to always be below experimental observations. On the other hand, with these same parameter but for micropillar sizes above $D = 1.0\,\mu m$, the computed flow strength is observed to be on the lower end or slightly below experimental observations.

Size scaling from the present computations is in good agreement with a wide range of experimental observations, with an exponent of -0.69. This is in close agreement with the exponent produced by the experimental results produced by Frick et al. (2008), which is equal to -0.69, and those reported by Dimiduk et al. (2005), which is equal to -0.64.

5. Size effects on work-hardening

A number of factors can contribute to the observed size effects on the work-hardening of micropillars. Some possible factors are cross-slip activation, crystal rotation, or large deformation. Up till now, no detailed investigation has been performed to understand the influence of these factors on the work-hardening of micropillars. In the following, we perform simulations to shed light on the influence of cross-slip activation on the observed hardening of micropillars.

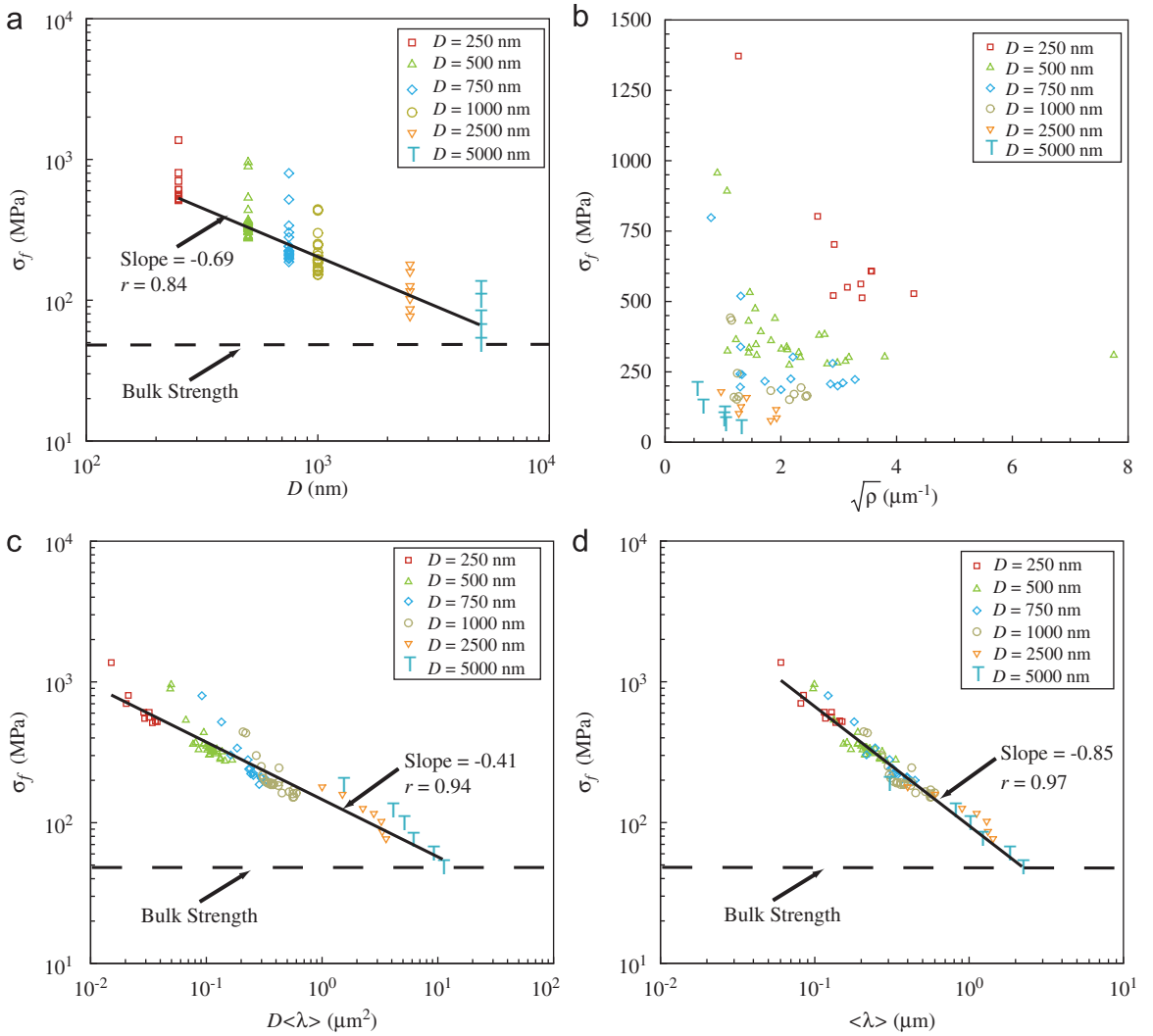

Fig. 9. Statistical results for the flow strength at 0.5% strain vs. (a) micropillar diameter; (b) square root of the dislocation density at the onset of plastic flow; (c) micropillar diameter multiplied by the average activated dislocation length over the initial dislocation density; (d) average activated dislocation length.

5.1. *Effect of cross-slip activation*

It is clear from the above results that after the flow strength is reached, no work hardening is observed. On the other hand, some experimental observations indicate that the strain hardening rate increases as the micropillar size decreases (Volkert and Lilleodden, 2006; Frick et al., 2008). Until now, the activated dislocation link length mechanism fails to predict this behavior, which indicates that other mechanisms come into play in the work-hardening regime. One of these mechanisms that have not been considered yet is cross-slip activation.

Dislocation cross-slip is generally recognized to have an important role in several aspects of material deformation. Cross-slip not only influences substructure morphology and evolution, but it is also known to control stage-III work-hardening in bulk metals. While there are several studies and proposed mechanisms of cross-slip (Schoeck and Seeger, 1955; Friedel, 1957; Escaig, 1968), it remains one of the lesser understood aspects of plastic deformation.

For the consideration of cross-slip in our current BEM-PDD method, we adopt the stochastic probabilistic model developed by Kubin et al. (1992) for discrete DD simulations. This model is based on the Friedel–Escaig (Friedel, 1957; Escaig, 1968) mechanism of thermally activated cross-slip. In this mechanism the original screw dislocation dissociates into a pair of Schockley partials on its glide plane, constricts at one point and then immediately redissociates on the cross-slip plane. In this mechanism the calculated activation enthalpies and volumes seem to be in fair agreement with experimental data (Bonneville and Escaig, 1979), with recent continuum calculations based on the self-stress method (Duesbery et al., 1992), and with atomistic simulations (Rasmussen et al., 1997).

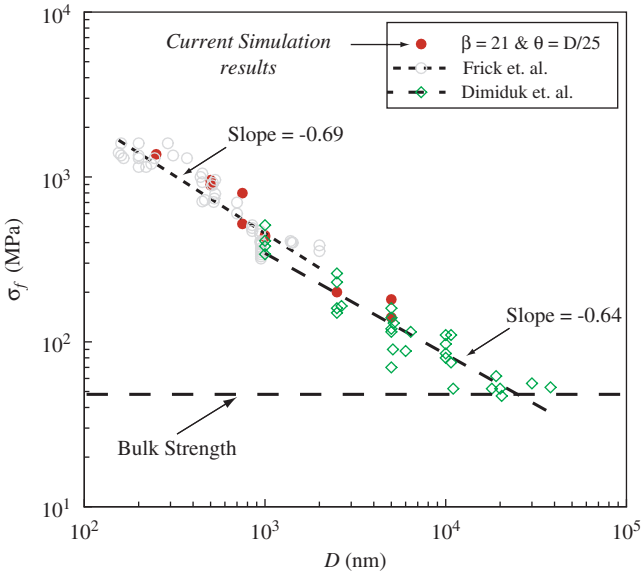

Fig. 10. Statistical results of the flow strength vs. micropillar diameter from experiments (Dimiduk et al., 2005; Frick et al., 2008) and current computer simulations.

Following Kubin et al. (1992), the probability P of cross-slip of a screw segments of length L is calculated as follows:

$$P = \beta \frac{L}{L_0}\frac{\delta t}{t_0}\exp\left(\frac{\tau_d - \tau_{\mathrm{III}}}{k_{\mathrm{B}}T}V\right), \tag{11}$$

where β is a normalization coefficient ensuring that $P \in [0,1]$, k_{B} is the Boltzmann constant, $T = 300\,\mathrm{K}$ is the simulation temperature, τ_{III} is the critical resolved shear stress at the onset of stage III of plastic deformation and is 55 MPa for FCC Ni in accordance with experimental values (Mader, 1963; Starenchenko et al., 1999), V is the activation volume and is a function of both the activation energy of cross-slip, which is equal to 2.35 eV (Rao et al., 1999) and τ_{III}, and is calculated here to be equal to $V = 420b^3$, with b the magnitude of the Burgers vector at room temperature. Finally, $L_0 = 1\,\mu\mathrm{m}$ and $t_0 = 1\,\mathrm{s}$ are reference length and time, respectively.

In our simulations, we define a screw dislocation segment as one with line direction that is aligned within 10° of the Burgers vector direction. A Monte-Carlo stochastic approach is utilized to determine if cross-slip is activated for screw dislocation segments, and is described as follows. At every time step, the probabilities for cross-slip of all screw segments are evaluated using Eq. (11). For each screw segment, a random number N between 0 and 1 is then generated. The calculated probability of the corresponding screw segment is compared with N, and the dislocation cross-slip takes place when $P > N$.

In Fig. 11, the engineering stress–strain responses of three micropillar sizes $D = 0.50, 0.75$, and $1.00\,\mu\mathrm{m}$ are shown, respectively. The compression loading follows the high-load sensitivity technique. Results of simulations with (solid lines) and without cross-slip activation (dashed-dot-dot lines) are shown. From these results, distinct jumps in the stress–strain curves are observed, between which the material behaves elastically.

The effect of cross-slip activation on the step formation is explained as follows. When the resolved shear stress on the cross-slip plane of the screw segments of an activated dislocation link is much greater than on its original plane, the screw segment will cross-slip and thus, the length of the initial dislocation link length will be reduced. Since both the cross-slipped segment as well as the rest of the dislocation left on the original plane will have a smaller length than the original length, a higher stress is needed to activate these new sources and thus an increase in the strength is observed. The dislocation microstructure evolution in both cases is shown in Fig. 12. It is observed that the activation of cross-slip leads to an increase in the dislocation density as well as a reduction of the average size of activated dislocation lengths.

In Fig. 13, the engineering stress–strain response of the same micropillars with the low-load sensitivity technique is shown. Results from both simulations with (solid lines) and without cross-slip activation (dashed-dot-dot lines) are shown. Again, from these results, distinct jumps in the stress–strain curves are observed.

Fig. 14 shows the FFT power versus period for two micropillar sizes $D = 0.5$ and $1.0\,\mu\mathrm{m}$ having the stress–strain relations shown in Fig. 11. The effect of cross-slip activation on the intermittency of the stress–strain curves is shown. A prominent cycle at a large period (about 5000 ns) is observed in both sizes when cross-slip is activated. This indicates that an avalanche-type instability is taking place periodically, in a manner reminiscent of a Hopf bifurcation (Ananthakrishna, 2007). This is only a conjecture at this point without rigorous analysis of the collective dynamics.

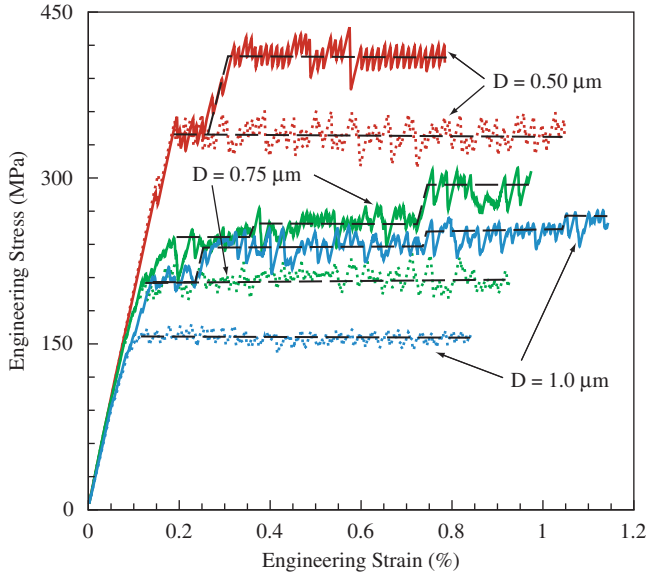

Fig. 11. Selected engineering stress versus engineering strain responses for different micropillar sizes using the high-load sensitivity technique. The solid lines are for simulations with cross-slip activation while the dotted lines are for simulations without cross-slip activation. Dashed lines represent the trend of the stress–strain curves.

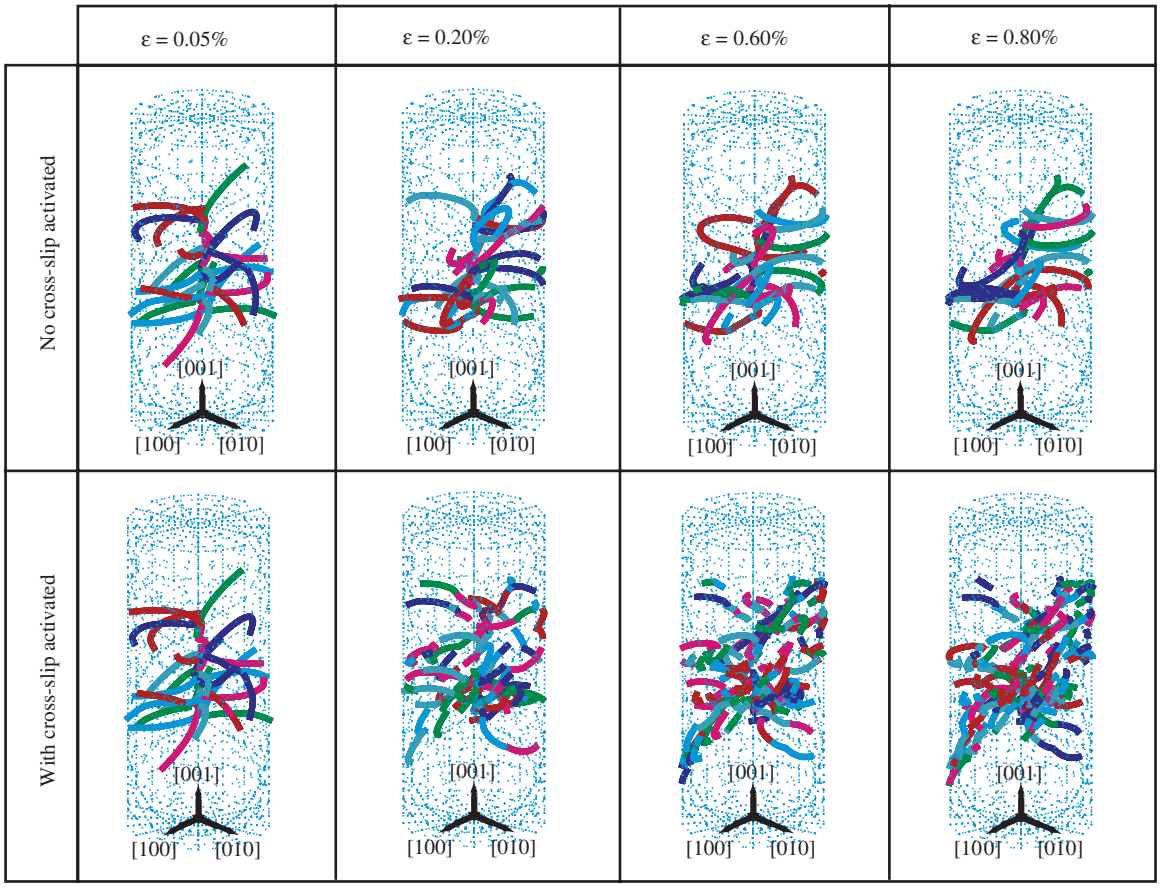

Fig. 12. Microstructure evolution with and without cross-slip activation for $D = 1.0\,\mu m$ with the high-load sensitivity technique applied.

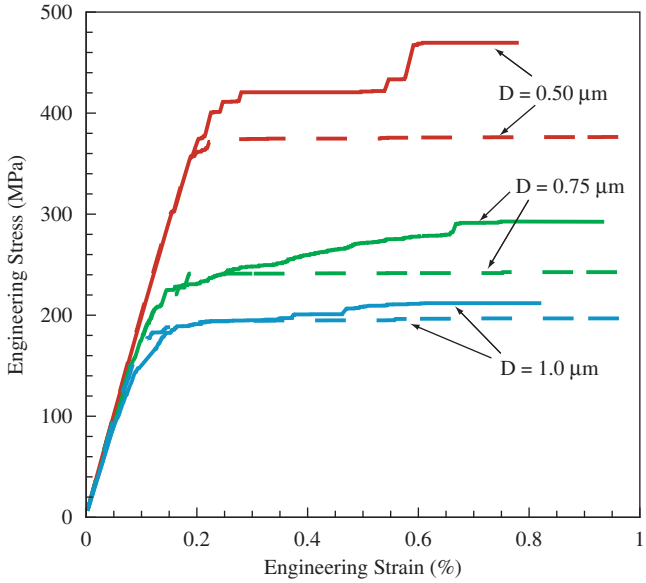

Fig. 13. Engineering stress versus engineering strain for different micropillar sizes using the low-load sensitivity technique. The solid lines are with cross-slip activation while the dashed lines are without cross-slip activation.

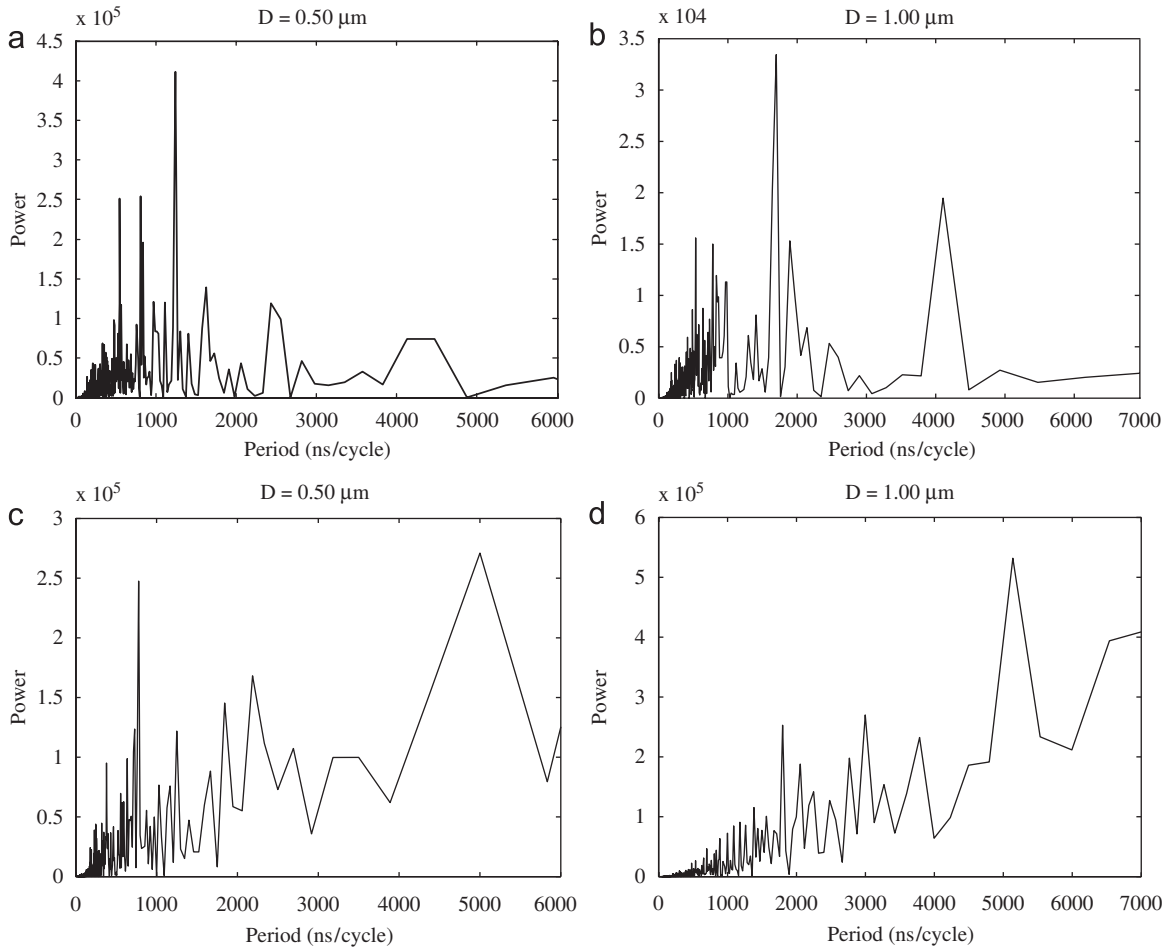

Fig. 14. FFT power versus period for the dislocation density of two different micropillar sizes. In (a) and (b) cross-slip is not activated while in (c) and (d) cross-slip is activated.

6. Discussion and conclusions

The current statistical investigation of the stress–strain behavior of single-crystal Ni micropillars oriented for multi-slip using three-dimensional dislocation dynamics modelling revealed several important aspects of the effects of size and initial dislocation source distribution on the flow strength and work-hardening. With the increased interest in micropillar compression tests, and the existence of some conflicting test results, dislocation dynamics modelling is utilized as an aid to a mechanistic interpretation of experimental observations. Because computer simulations can be performed without the complications arising from experimental setups. The current simulations examine various possibilities and mechanisms regarding the origin of the observed size effects on plastic flow and work-hardening.

One of the ideas recently invoked to explain the observed size effects is the dislocation starvation mechanism suggested by Greer et al. (2005). In this hypothesis, it is assumed that dislocations exit the pillar surface before the possibility of multiplication or dislocation interactions. Thus, the dislocation density drops, and high stresses are required to nucleate new dislocations (Greer et al., 2005; Greer and Nix, 2006; Greer, 2006). In the current simulations, however, when an initial dislocation density of pinned dislocations (either single- or double-ended) is introduced as an initial microstructure, no drop in the dislocation density is observed after the onset of plastic flow. Although surface image forces are accounted for in the present simulations, dislocations do not escape, as suggested by the starvation mechanism. Any form of internal or external end pinning, which is highly likely in pillars containing an initial dislocation microstructure, leads to continuous regeneration of escaped dislocations. This suggests that the dislocation starvation mechanism is not operative under the conditions we investigated here.

Norfleet et al. (2008) observed that micropillars having sizes below 5 μm evolve a lower-bound dislocation density during deformation that is, on average, in excess of their expected average initial density, with an apparent trend that the average density increases with decreasing microcrystal size. On the other hand, in the original starvation scenario, one might expect to observe dislocation densities in deformed samples that are equal to or less than the initial dislocation density. Thus, the hypothesis that the increase in strength of microcrystals can be solely attributed to dislocations leaving the microcrystal (Greer et al., 2005) is contradicting the close examination of the dislocation density measurements in conjunction with measurements of initial dislocation content. In addition, Norfleet et al. (2008) concluded that, in their micropillar samples, the dislocation structure may have relatively effective dislocation pinning and a reduced number of weak-link dislocation sources, which is in agreement with our initial assumptions and results.

Based on the results presented here, one can still explain the experimentally observed size effects on both the flow strength and work-hardening on the basis of a "weakest-link activation mechanism". Within the framework of this proposed mechanism, we discuss three different experimental possibilities for the effect of the initial dislocation density on the flow strength of micropillars. These are: (1) the existence of an initial dislocation link-length distribution; (2) the existence of an initial surface damage layer in the pillar due to FIB processing; and (3) a pristine, damage-free micropillar.

Mughrabi (1976) experimentally determined the statistical distribution of pinned dislocation lengths in bulk FCC Cu, deformed in tension, as shown in Fig. 15. The normalized distribution that best fits these experimental results is also shown (solid line). Let us now assume that the micropillars are processed from a bulk crystal that has a similar distribution function. If the pillar diameter is greater than or equal to 2.0 μm, then the distribution will not change. On the other hand, if the pillar had a diameter smaller than 2.0 μm, then this distribution function should be renormalized. As an example, for a

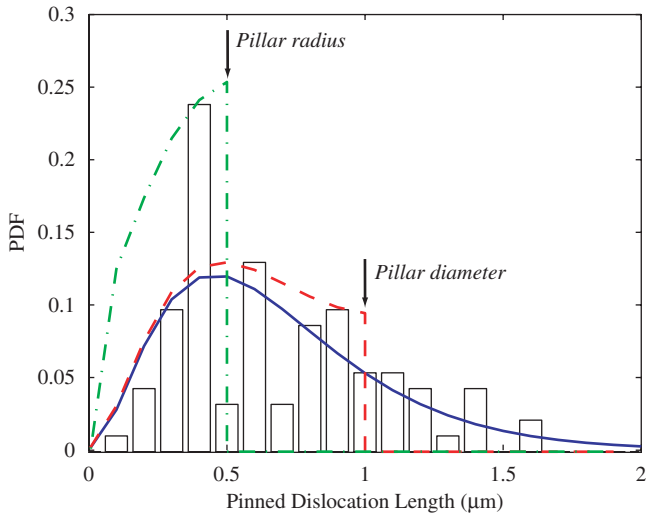

Fig. 15. Probability distribution function of pinned dislocation link-length. The hysterogram represents the experimentally measured distribution for Cu deformed in tension based on 92 evaluated segments (Mughrabi, 1976); the solid line is the corresponding normalized distribution; the dashed line is the normalized distribution for $D = 1.0\,\mu m$ before deformation; and the dash-dot line is the effective normalized distribution for $D = 1.0\,\mu m$.

pillar having a diameter of 1.0 μm, the dislocation link length distribution will be similar to the dashed line shown in Fig. 15. Also, the dislocations in the pillar will either be double-pinned, single-pinned, or surface-pinned.

As the stress increases in the micropillar, surface-pinned dislocations will be activated first. Since these dislocations are not pinned in the interior of the pillar they will expand and leave the pillar. Segments that are larger than the radius of the pillar will then be activated at relatively higher stress levels. After the activation of these segments, they will expand until they get pinned on the surface with lengthes less than or equal to the radius of the pillar (El-Awady et al., 2008). Thus, higher stresses will be required to activate the new dislocation distribution and the stress will increase elastically until the strength needed to activate the segments having lengths equal to the radius of the pillar is reached. Thus, the effective normalized distribution of the dislocation lengths in the pillar would be as shown in Fig. 15.

The flow strength required to activate the effective normalized distribution is the bottom data points in Fig. 9(a), which were calculated using an initial Weibull distribution having parameters $\beta = 15$ and $\theta = D/2$. It should be noted that this distribution gives the lower bound of the flow strength computed for any micropillars having size less than $D = 4.0\,\mu m$. For micropillars having sizes greater than $D = 4.0\,\mu m$, the dislocation distribution will be the same as that of a bulk crystal and in turn the computed flow strength will be similar. It should be observed that the flow strength calculated here using this distribution is somewhat smaller than the experimentally calculated flow strength of Dimiduk et al. (2005) and Frick et al. (2008)). This suggests that the dislocation link length distribution in these experiments is limited to even smaller sizes.

In-situ experiments (Shan et al., 2007) have shown that for micropillars having sizes below 0.16 μm, the initial dislocation density was completely driven out of the pillar by the applied compression loading. This is in agreement with the dislocation-starvation hypothesis. On the other hand, for larger pillars, it was observed that dislocations are not completely driven out of the pillar, and that they are observed throughout the deformation process. This can be interpreted within our model as follows. The probability of a single-pinned or double-pinned dislocation of length 0.1 μm existing in the interior of a micropillar is very small. Thus, for a micropillar having a diameter $D = 0.16\,\mu m$ or smaller, most pre-existing dislocations will be surface pinned dislocations. Also, for such small sizes, the probability of having more than a couple of dislocations will be very small. Thus junction formation would be very unlikely, and these surface-pinned dislocations would escape from the micropillar leaving it dislocation free, and the dislocation-exhaustion hypothesis would be possible for such small submicron pillar sizes. On the other hand, for larger pillars there is a higher probability of having single- and/or double-pinned dislocations in the pillar interior, and thus the dislocation-starvation mechanism would not be expected to dominate.

Another important point to consider in our discussion here is the effect of the existence of an initial damage layer in the pillar due to FIB processing. It is well acknowledged that the FIB process introduces a damaged surface due to ion bombardment. It was suggested that this damage layer may alter the mechanical properties and the deformation behavior compared to undamaged samples (Kiener et al., 2006, 2007). The damage was reported to be in the form of dislocations decorated with Ga, vacancy clusters in the form of stalking fault tetrahedra, Ga-based precipitates, dislocation networks, and dislocation loops that have resulted from the collapse of the vacancy clusters (Kiener et al., 2007). The penetration depth was reported to be 50 nm from the surface of the pillar.

It was suggested by Shan et al. (2007), especially for micropillar sizes $D = 0.16\,\mu m$ and smaller, that this implanted damage escapes the pillar. For larger size pillars, on the other hand, most of the initial dislocation density was not completely driven out of the pillar. This suggests that there is a possibility of interaction between surface damage and pinned dislocations in the pillar.

In the context of our current model, such a damage layer will significantly affect the pinned dislocation length distribution. Assuming a micropillar having size $D = 0.25\,\mu m$, and a surface-pinned dislocation having length equal to the radius of the pillar of ($\lambda = 0.125\,\mu m$). If this dislocation interacts with the damage layer at a depth of 50 nm, will most likely get pinned resulting in a new dislocation configuration with lengths of 50 and 75 nm. Thus, the dislocation is almost split in half, and the strength of the pillar will increase dramatically to be able to activate the new dislocation length distribution. This new length distribution is in agreement with the initial distribution used for the highest flow strength calculated for a micropillar size $D = 0.25\,\mu m$, as shown in Fig. 9(a), where $\theta = D/8$, and the calculated flow strength falls within the experimental range. Thus, it is possible that the interaction of pre-existing dislocations in the pillar with this damage layer can result in further pinning of dislocations, which would reduce the effective dislocation length and thus increase the flow strength.

Finally, let us now consider the situation of dislocation-free micropillars. In this case, the pillar is free from any pre-existing dislocations or damaged layer. Since there is no initial dislocation structure in the pillar to support plastic flow, the strength will increase until the applied stress reaches the critical stress needed to nucleate dislocations. This was experimentally observed for molybdenum single-crystal micropillars free from dislocations that were prepared by chemical etching (Bei et al., 2007a,b), as opposed to the FIB process. In these experiments, all tested micropillars having sizes 0.36–1.0 μm yielded shear strengths close to the theoretical value.

On the other hand, within the framework of the "weakest-link activation mechanism", the observed size effects on work-hardening can result from a number of factors. The first possibility is cross-slip activation, which we examined here. Cross-slip will result in the reduction of the length of previously activated segments, and thus higher stresses would be required to activate other pinned dislocations having smaller lengths. Since the probability of having sources with a long link length is higher in larger size pillars, the effect of cross-slip on hardening would be more significant for smaller crystals. This can be observed by comparing the magnitude of the step jumps in Figs. 11 and 13.

A second possibility that has not been addressed is the effect of crystal rotation during deformation. Although there are conflicting experimental observations on crystal rotations, FEM simulations shows pronounced deformation-induced orientation changes that takes place at compressive strains of about 0.2 (Raabe and Roters, 2007). This can have an important effect on reducing the critical resolved shear stress on the slip plane of previously activated dislocations (i.e. geometric softening), which could result in its deactivation. Thus, higher stresses would be needed to activate sources on previously un-activated slip systems.

A final possibility that can contribute to the observed increase in hardening is the dramatic change in crystal geometry. This effect would mainly be observed in single-crystals deforming in single-slip. As the micropillar continuously slips due to the activation of dislocation sources, the area that the dislocation sweeps till it reaches the pillar surface will be reduced, which would reduce the length of activated sources. Thus, at high strains, the activated dislocation length would dramatically change with a corresponding increase in the micropillar strength.

In summary, we performed here three-dimensional dislocation dynamics simulations of the compression of Ni single-crystal micropillars oriented for multi-slip. Plastic flow arises from the collective motion of dislocations within the volume of the micropillars. The effect of preventing the applied load from decreasing is investigated. In addition, a number of parameters and mechanisms (e.g. micropillar size, average length of activated single-pinned dislocations, and cross-slip activation) are examined in an effort to identify size scaling aspects of plastic flow and work-hardening. The simulation results are in general agreement with several experimental observations. The size effects on the flow strength and work-hardening are clearly observed. It is also observed that plastic flow is intermittent and not continuous. The size effects on the flow strength are rationalized here on the basis of a statistical variation in the length of single-pinned dislocation sources in the crystal. In addition, a number of scaling laws that relate the flow strength to the micropillar diameter, and the average length of activated single-pinned dislocations were developed. The dislocation density evolution is observed to be cyclic and a FFT analysis revealed that dislocation activities in the volume are cyclical as well. In addition, the activation of cross-slip is shown to have a significant effect on work-hardening. Finally, the observed size effects are shown to be consistent with a ‘‘weakest-link activation mechanism’’.

Acknowledgements

We acknowledge the support of the U.S. Air Force Office for Scientific Research (AFOSR), through Grant No. FA9550-07-1-0396, with UCLA.

References

Ananthakrishna, G., 2007. Current theoretical approaches to collective behavior of dislocations. Phys. Rep. 440 (4–6), 113–259.
Basinski, S., Basinski, Z., 1979. Plastic deformation and work hardening. In: Nabarro, F. (Ed.), Dislocations in Solids, 4. North-Holland, Amsterdam, pp. 261–362.
Bei, H., Shim, S., George, E., Miller, M., Herbert, E., Pharr, G., 2007a. Compressive strengths of molybdenum alloy micropillars prepared using a new technique. Scripta Mater 57 (5), 397–400.
Bei, H., Shim, S., Miller, M., Pharr, G., George, E., 2007b. Effects of focused ion beam milling on the nanomechanical behavior of a molybdenum-alloy single crystal. Appl. Phys. Lett. 91, 111915.
Benzerga, A., Shaver, N., 2006. Scale dependence of mechanical properties of single crystals under uniform deformation. Scripta Mater 54 (11), 1937–1941.
Bonneville, J., Escaig, B., 1979. Cross-slipping process and the stress-orientation dependence in pure copper. Acta Metall 27 (9), 1477–1486.
Budiman, A., Han, S., Greer, J., Tamura, N., Patel, J., Nix, W., 2008. A search for evidence of strain gradient hardening in Au submicron pillars under uniaxial compression using synchrotron x-ray microdiffraction. Acta Mater 56, 602–608.
Deshpande, V., Needleman, A., Van der Giessen, E., 2005. Plasticity size effects in tension and compression of single crystals. J. Mech. Phys. Solids 53 (12), 2661–2691.
Dimiduk, D., Koslowski, M., LeSar, R., 2005. Size-affected single-slip behavior of pure nickel microcrystals. Scripta Mater 53 (15), 4065–4077.
Duesbery, M., Louat, N., Sadananda, K., 1992. The mechanics and energetics of cross-slip. Acta Metall. Mater. 40 (1), 149–158.
El-Awady, J.A., Biner, S.B., Ghoniem, N.M., 2008. A self-consistent boundary element, parametric dislocation dynamics formulation of plastic flow in finite volumes. J. Mech. Phys. Solids 56 (5), 2019–2035.
Escaig, B., 1968. Cross-slipping process in the fcc structure. In: Rosenfield, A., Hahn, G., Bement, Jr., A., Jaffee, R. (Eds.), Proceedings of the Battelle Colloquium in Dislocation Dynamics. McGraw- Hill, New York.
Foreman, A., 1967. The bowing of a dislocation segment. Phil. Mag. 15 (137), 1011–1021.
Frick, C., Clark, B., Orso, S., Schneider, A., Arzt, E., 2008. Size effect on strength and strain hardening of small-scale [111] nickel compression pillars. Mat. Sci. Eng. A 489 (1–2), 319–329.
Friedel, J., 1957. In: Fisher, J., Johnston, W., Thromson, R., Vreeland, T. (Eds.), Dislocations and mechanical properties of crystals. Wiley, New York, pp. 330–332.
Ghoniem, N., Sun, L., 1999. Fast sum method for the elastic field of 3-D dislocation ensembles. Phys. Rev. B 60 (1), 128–140.
Ghoniem, N., Tong, S.-H., Sun, L., 2000. Parametric dislocation dynamics: a thermodynamics-based approach to investigations of mesoscopic plastic deformation. Phys. Rev. B 61 (2), 913–927.
Greer, J., 2006. Bridging the gap between computational and experimental length scales: a review on nano-scale plasticity. Rev. Adv. Mater. Sci. 13, 59–70.
Greer, J., Nix, W., 2006. Nanoscale gold pillars strengthened through dislocation starvation. Phys. Rev. B 73, 245410.
Greer, J., Oliver, W., Nix, W., 2005. Size dependence of mechanical properties of gold at the micron scale in the absence of strain gradients. Acta Mater 53 (6), 1821–1830.
Greer, J., Weinberger, C., Cai, W., 2008. Comparing the strength of fcc and bcc sub-micron pillars: compression experiments and dislocation dynamics simulations. Mater. Sci. Eng. A 493 (1–2), 21–25.
Guruprasad, P., Benzerga, A., 2008. Size effects under homogeneous deformation of single crystals: a discrete dislocation analysis. J. Mech. Phys. Solids 56 (1), 132–156.

Kiener, D., Motz, C., Schöberl, T., Jenko, M., Dehm, G., 2006. Determination of mechanical properties of copper at the micron scale. Adv. Eng. Mater 8 (11), 1119–1125.
Kiener, D., Motz, C., Rester, M., Jenko, M., Dehm, G., 2007. Fib damage of Cu and possible consequences for miniaturized mechanical tests. Mater. Sci. Eng. A 459, 262–272.
Kubin, L., Canova, G., Condat, M., Devincre, B., Pontikis, V., Bréechet, Y., 1992. Dislocation microstructures and plastic flow: a 3-D simulation. Diffusion and Defect Data - Solid State Data, Part B (Solid State Phenomena) 23–24, 455–472.
Maaß, R., Van Petegem, S., Grolimund, D., Van Swygenhoven, H., Uchic, M., 2007a. A strong micropillar containing a low angle grain boundary. Appl. Phys. Lett 91, 131909.
Maaß, R., Van Petegem, S., Van Swygenhoven, H., Derlet, P., Volkert, G., Grolimund, D., 2007b. Time-resolved laue diffraction of defoming micropillars. Phys. Rev. Lett 99, 145505.
Mader, S., 1963. Surface and thin-foil observations of the substructure in deforrmed face-centered cubic and hexagonal close-packed metal single crystals. In: Thomas, G., Washburn, J. (Eds.), Electron Microscopy and strength of crystals. Interscience publishers, p. 183.
Mughrabi, H., 1976. Observation of pinned dislocation arrangements by transmission electron microscopy (TEM). J. Microsc. Spectrosc. Electron 1, 571–584.
Norfleet, D., Dimiduk, D., Polasik, S.J., a, U.M., Mills, M., 2008. Dislocation structures and their relationship to strength in deformed nickel microcrystals. Acta Mater 56 (13), 2988–3001.
Parthasarathy, T., Rao, S., Dimiduk, D., Uchic, M., Trinkle, D., 2007. Contribution to size effect of yield strength from the stochastics of dislocation source lengths in finite samples. Scr. Mater 56 (4), 313–316.
Puschl, W., Frydman, R., Schoeck, G., 1982. The strength of the dislocation forest for 30° and 60° dislocations. Phys. Stat. Sol. (a) 74, 211–216.
Raabe, D., M.D., Roters, F., 2007. Effects of initial orientation, sample geometry and friction on anisotropy and crystallographic orientation changes in single crystal microcompression deformation: A crystal plasticity finite element study. Acta Mater. 55(13), 4567–4583.
Rao, S., Parthasarathy, T., Woodward, C., 1999. Atomistic simulation of cross-slip processes in model fcc structures. Phil. Mag. A 79 (5), 1167–1192.
Rasmussen, T., Jacobsen, K.W, Leffers, T., Pedersen, O.B., Srinivasan, S.G., Jónsson, H., 1997. Atomistic determination of cross-slip pathway and energetics. Phys. Rev. Lett 79 (19), 3676–3679.
Schoeck, G., Frydman, R., 1972. The contribution of the dislocation forest to the flow stress. Phys. Stat. Sol. (b) 53, 661–673.
Schoeck, G., Seeger, A., 1955. Activation energy problems associated with extended dislocations. In: Report of the Bristol Conference on Defects in Crystalline Solids. Physical Society, London, pp. 340–346.
Shan, Z., Mishra, R., Asif, S., O.L., W., Minor, A., 2007. Mechanical annealing and source-limited deformation in submicrometre-diameter Ni crystals. Nature Materials 7, 115–119.
Starenchenko, V., Lychagin, D., Shaekhov, R., Kozlov, a., 1999. Action of test temperature on evolution of dislocation structure of nickel single crystals with the [001] compression axis. Russian Physics J. 42 (7), 653–659.
Takahashi, A., Ghoniem, N., 2008. A computational method for dislocation-precipitate interaction. J. Mech. Phys. Solids 56 (4), 1534–1553.
Tang, H., Schwarz, K., Espinosa, H., 2007. Dislocation escape-related size effects in single-crystal micropillars under uniaxial compression. Acta Mater 55 (5), 1607–1616.
Tang, H., Schwarz, K., Espinosa, H., 2008. Dislocation-source shutdown and the plastic behavior of single-crystal micropillars. Phys. Rev. Lett. 100, 185503.
Uchic, M., Dimiduk, D., Florando, J., Nix, W., 2003. Exploring specimen size effects in plastic deformation of Ni_3(Al,Ta). In: George, E. (Ed.), Materials Research Society Symposium Proceedings. Vol. 753. Materials Research Society, Pittsburgh, PA, pp. BB1.4.1—BB1.4.6.
Uchic, M., Dimiduk, D., Florando, J., Nix, W., 2004. Sample dimensions influence strength and crystal plasticity. Science 305, 986–989.
Uchic, M., Dimiduk, D., 2005. A methodology to investigate size scale effects in crystalline plasticity using uniaxial compression testing. Mat. Sci. Eng. A 400-401, 268–278.
Van der Giessen, E., Needleman, A., 1995. Discrete dislocation plasticity: a simple planar model. Modeling Simul. Mater. Sci. Eng. 3 (5), 689–735.
Volkert, C., Lilleodden, E., 2006. Size effects in the deformation of sub-micron au columns. Philos. Mag. 86 (33–35), 5567–5579.
von Blanckenhagen, B., Arzt, E., Gumbsch, P., 2004. Discrete dislocation simulation of plastic deformation in metal thin films. Acta Mater. 52, 773–784.
Weygand, D., Poignant, M., Gumbsch, P., Kraft, O., 2007. Three-dimensional dislocation dynamics simulation of the influence of sample size on the stress–strain behavior of fcc single-crystalline pillars. Mater. Sci. Eng. A 483–484, 188–190.
Zhu, T., Li, J., Samanta, A., Leach, A., Gall, K., 2008. Temperature and strain-rate dependence of surface dislocation nucleation. Phys. Rev. Lett. 100, 025502.